Addition and elimination reactions of 2 in ruthenaborane clusters: A computational study

Hassan Rabaâ, Sundargopal Ghosh, Dage Sundholm, Jean-François Halet, Jean-Yves Saillard

Addition and elimination reactions of H_2 in ruthenaborane clusters: A computational study

Hassan Rabaâ [a,*], Sundargopal Ghosh [b], Dage Sundholm [c], Jean-François Halet [d,e], Jean-Yves Saillard [d,e]

[a] *Département de Chimie, ESCTM, Université Ibn Tofail, P.O. Box. 133, Kénitra 14000, Morocco*
[b] *Department of Chemistry, Indian Institute of Technology Madras, Chennai 600 036, India*
[c] *Department of Chemistry, P.O.B. 55 (A.I. Virtasen aukio 1), FIN-00014, University of Helsinki, Finland*
[d] *Institut des Sciences Chimiques de Rennes, UMR 6226 CNRS-Université de Rennes 1, F-35042 Rennes Cedex, France*
[e] *Université Européenne de Bretagne, 5 Boulevard Laënnec, F-35000 Rennes, France*

A B S T R A C T

Ruthenaborane clusters have been modelled by performing density functional theory calculations using the B3LYP functional. The calculations gain insights into hydrogen storage and the H–H bond activation by ruthenaboranes. To study the nature of the chemical bond of H_2 molecules attached to ruthenaboranes, we carried out structural optimizations for different ruthenaborane clusters and determined transition state structures for their hydrogenation addition/elimination reactions. Calculations of the reaction pathways yielded different transition-state structures involving molecular hydrogen bonded to the cluster or formation of metal hydrides. The H–H bond of H_2 seems to be activated by the ruthenaborane clusters as activation energies of 24–42 kcal/mol were calculated for the H_2 addition reaction. The calculated Gibbs free energy for the H_2 addition reaction is 14–27 kcal/mol. The calculated activation energies and the molecular structures of the $[(C_5Me_5)Ru_2B_{10}H_{16}]$, $[(C_5Me_5)Ru_2B_8H_{14}]$ and $[(C_5Me_5)Ru_2B_8H_{12}]$ clusters with different degree of hydrogenation are compared. The mechanisms of the H_2 addition and elimination reactions of the studied clusters suggest that they might be useful as hydrogen storage materials due to their ability to activate the H–H bond. They also serve as an example of the ability of hypoelectronic metallaboranes to reversibly or irreversibly bind hydrogen.

Introduction

During the last decade, storage of molecular hydrogen has become an important research field in industry as well as in academia [1–6]. Several of the fundamental and applied studies have focused on the use of metal hydrides as materials for hydrogen storage [2]. Research efforts have been put on the development of new materials with tunable thermodynamic and kinetic properties with the aim of improving the hydrogenation–dehydrogenation properties of hydrogen-storage materials [1–3,5]. The main challenge is to store hydrogen and to use it as industrial battery fuel in combustion engines by employing borohydrides or metal hydrides such as MgH_2 and $LiNH_2$, considered as clean energy technologies [2–6]. Some prerequisites for useful recyclable hydrogen-storage materials are fast hydrogen uptake and release reactions as well as high structural stability during the repeated hydrogen recycling process. In addition, the hydrogen storage material must not be too expensive to be useful in large scale applications [6]. Recent studies have focused on mixtures of complex metal hydrides as potential hydrogen storage materials. Yang et al. found that ternary mixtures of MgH_2, $LiNH_2$ and $LiBH_4$ have increased the hydrogen release as compared to binary mixtures of these compounds [7]. The magnesium borohydride $Mg(BH_4)_2$ is also a promising material for hydrogen storage because of its high gravimetric storage capacity of 15.0 mass% H_2 [3,6–13].

The enthalpy of a reversible reaction of dihydrogen uptake/release of a metal hydride material should be lower than ~20 kcal/mol of H_2 assuming moderate heating [4]. This thermodynamical condition does not preclude the necessity for a low activation energy allowing the reaction to proceed under moderate temperature.

In previous studies [14,15], it was discovered that some electron-deficient metallaboranes have the ability to bind a very large amount of hydrogen. It was suggested that reversible dihydrogen uptake by such clusters under very mild conditions should be

* Corresponding author. Tel.: +212 537 375 506.
E-mail address: hrabaa@yahoo.com (H. Rabaâ).

possible [3,8–17] making them a promising starting point for designing new hydrogen storage materials [3,11,13–19].

The activation of the H–H bond of H_2 is analysed in this study, as a continuation on previous studies where it was shown that an electron-deficient coordination mode seems to be responsible for the activation of H–H bonds [21]. The activation of σ (H–H, C–H and B–H) bonds is of central interest in homogeneous or heterogeneous catalysis, where it has been the leitmotiv in the past decades [19–22]. The chemistry of the dihydrogen bonding including aspects of hydrogen storage has been reviewed by Kubas [20]. Studies on bis-dihydrogen-ruthenium complexes such as $(PCy_3)_2RuH_2(H_2)_2$ demonstrated that there is an excellent balance between σ-donation and π back-donation when binding labile dihydrogen ligands to the complex [23–25].

In this work, we study the H_2 addition/elimination reactions on the hydrogen-rich ruthenaborane $Cp^*_2Ru_2B_{10}H_{16}$ (**1**) [14], $Cp^*_2Ru_2B_8H_{14}$ (**2**) and $Cp^*_2Ru_2B_8H_{12}$ (**3**) ($Cp^* = C_5Me_5$) [16] clusters experimentally characterized by one of us. The aim of this computational study is to provide a deeper understanding of the electronic structures of these metallaboranes and to predict how molecular hydrogen can coordinate to the cluster cage. Reaction coordinate profiles of the hydrogenation and dehydrogenation mechanism have been computationally studied at the B3LYP level of theory for estimating the energy barriers and the Gibbs free energy of the reactions and for predicting the feasibility of H_2 addition/elimination reactions.

Computational methods

Theoretical calculations were performed with the Gaussian 09 series of programs [26] at the density functional theory (DFT) level using the B3LYP functional [27–29]. To reduce computational efforts, the C_5Me_5 (Cp^*) ligands (see Chart 1) were replaced by C_5H_5 (Cp) (see Fig. 1).

The LANL2DZ relativistic pseudo-potential (ECP) were used for the ruthenium and the 6-311G++(d,p) basis sets for the H, B and C atoms. Harmonic vibrational frequencies were calculated for each cluster to characterize the stationary points on the potential energy surface. All stationary points obtained in the structure optimizations were found to be minima on the potential energy surface. The geometry optimizations were performed on spin-singlet states without any symmetry constraints. Transition-state (TS) structures were obtained by using the synchronous transit-guided quasi-Newton (STQN) method developed by Schlegel et al. as implemented in Gaussian 09 [30,31]. Using the intrinsic reaction coordinates (IRC) procedure, we checked that the transition states connect the relevant reactants and products [31]. Gibbs free energies were calculated by considering the entropy contributions obtained in the vibration frequency calculations.

Solvent effects on the activation energy were analysed by performing single-point calculations using the polarizable continuum model (PCM) model [32] and a dielectric constant (ε) of 2.374 corresponding to toluene.

Results and discussion

The structure of $Cp^*_2Ru_2B_{10}H_{16}$ (**1**) shown in Chart 1, is of C_{2v} symmetry. Its B_{10} framework has been described as deriving from a truncated tetrahedron having two missing vertices and of which two hexagonal faces are capped by the two metals atoms [14]. Whereas for this type of architecture one may expect a count of 17-skeletal-electron pair (sep) [33,34], the formal electron count of (**1**) is only 14 sep. Such an electron deficiency with respect to the standard cluster electron counting rules is not uncommon in this family of metallaboranes and has been rationalized in previous studies [17,33]. In addition, each of the ten boron atoms of (**1**) are linked to one terminal hydrogen and there are six hydrogens bridging boron atoms.

The experimental metrical data of the synthesized cluster $Cp^*_2Ru_2B_{10}H_{16}$ (**1**) are compared to the optimized bond distances of the C_{2v} model $Cp_2Ru_2B_{10}H_{16}$ (**A**) model in Table 1. The numbering of the atoms is shown in Chart 1. The calculated Ru–Ru′ distance of 4.105 Å is 5 pm longer than the experimental one of 4.057 Å [14]. The average B–B and Ru–B bond lengths of 1.844 Å and 2.191 Å are 2 pm and 5 pm longer than the experimental values, respectively. The six Ru–B bond lengths are in the range 2.155–2.266 Å and the mean distance between Ru and the six carbons of the Cp ring is 2.351 Å. The somewhat longer bond distances obtained in the calculations are not quite unexpected since the employed computational level tends to overestimate bond lengths [35,36].

The molecular orbital diagram of **A** is shown in the middle of Fig. 2. The highest occupied molecular orbital (HOMO) is mostly localized on the metal atoms. The lowest unoccupied molecular orbital (LUMO) is separated from the HOMO by 4.31 eV at the B3LYP level. This large HOMO–LUMO gap is consistent with the stability of the 14-sep cluster **1**. The LUMO ($3a_1$) as shown in Fig. 3 is extended all over the $B_{10}H_{16}$ moiety, whereas the HOMO ($2a_1$) is mainly localized on the metal atoms (see Fig. 2). The plot analysis indicates that the LUMO has a weak metal–ligand antibonding character with 67% on the borons and 33% on M–Cp moieties whereas the HOMO exhibits significantly more metallic character than the LUMO. The HOMO and the LUMO play a central role in the H_2 elimination/addition reactions as discussed in the next section.

*Reaction path for H_2 elimination in **A***

A large number of isomers can be envisaged by eliminating one H_2 molecule from **A**. The energetically most stable $Cp_2Ru_2B_{10}H_{14}$ cluster (see **B** in Fig. 3) corresponds to the elimination of the two adjacent hydrogen atoms H15 and H16 bridging the B5–B6 and B6–B7 bonds, respectively. The optimized bond distances of the structure **B** are given in Table 1. The elimination of H15 and H16 leads to changes of about 10 pm in the B6–B7 and B7–B8 distances, whereas the B5–B6 and B9–B10 distances are 3 pm longer in **B** than in **A**. The Ru–B distances are only slightly affected by the H_2 elimination (see Table 1).

The molecular orbital diagram of **B** in the left side of Fig. 3 shows a large HOMO–LUMO gap of 4.01 eV. The wide HOMO–LUMO gap indicates that **B** is a stable compound, even though it has two hydrogen atoms less and its 13 sep maintain the **A** structure.

The STQN method was employed to determine the reaction pathway between **A** and **B**. The STNQ calculation found one transition state **TS1** with one imaginary frequency (see Fig. 3). The starting point for the STQN was obtained by adding a dihydrogen molecule to **B** far away from the cluster. The STQN calculation converges to **TS1** which has a short H11–H12 bond distance of 0.801 Å bridging the B1–B2 and B4–B5 atoms. For **TS1**, the B1–B2 and B4–B5 bonds are 2.368 Å and 1.981 Å respectively. These bonds are significantly longer than for **B**, whereas the B7–B8 bond shrinks to 1.678 Å. For **TS1**, the B1H11 and B2H12 bonds are 2.066 Å and 1.538 Å. The Ru–Ru′ bond distance is practically unchanged (see Table 1). **TS1** has also a large HOMO–LUMO gap of 3.95 eV.

The energy profile for the elimination reaction of H_2 from **A** yielding **B** was computed via the IRC procedure (see Fig. 4). The calculated energy barrier of 28 kcal/mol is somewhat smaller than the energy barrier of 32 kcal/mol previously estimated for the reaction $Cp_2Re_2B_6H_{10} + H_2$ [15].

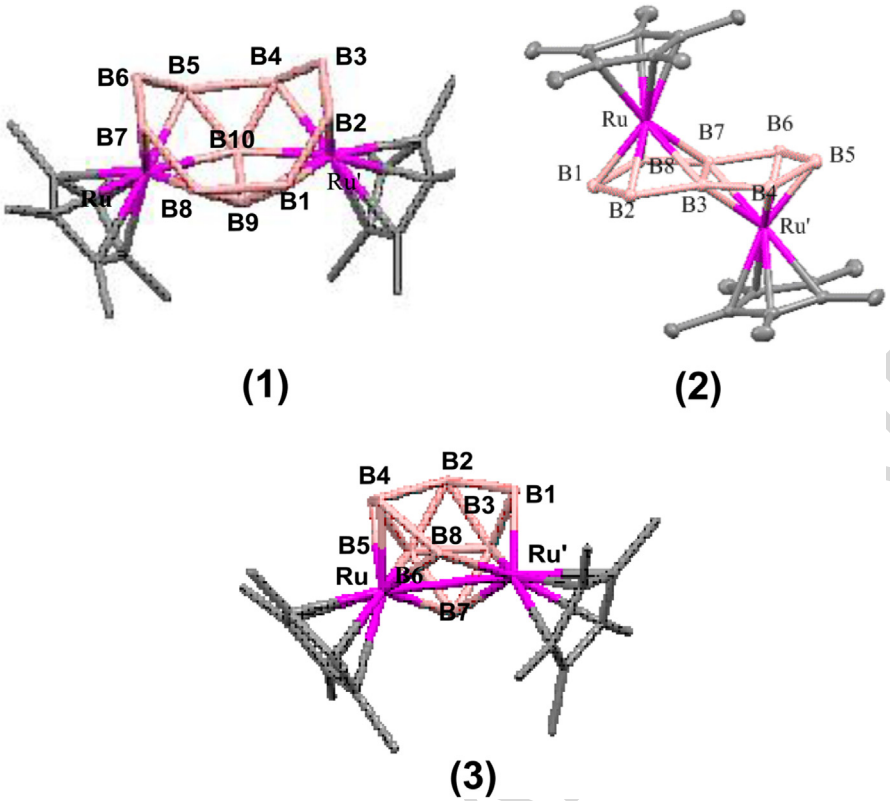

Chart 1. Labelling of the atoms for the studied clusters: $[Cp^*_2Ru_2B_{10}H_{16}]$ (**1**), $[Cp^*_2Ru_2B_8H_{14}]$ (**2**) and $[Cp^*_2Ru_2B_8H_{12}]$ (**3**).

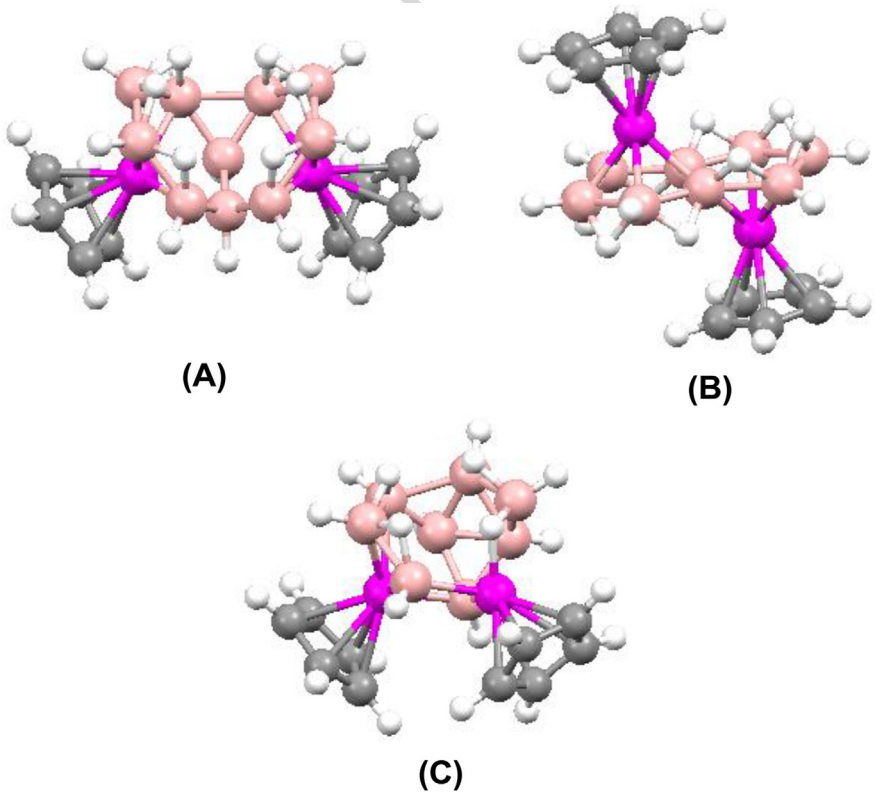

Fig. 1. Molecular structures of the studied model clusters: $[Cp_2Ru_2B_{10}H_{16}]$ (**A**), $[Cp_2Ru_2B_8H_{14}]$ (**B**) and $[Cp_2Ru_2B_8H_{12}]$ (**C**). The ruthenium atoms are shown in red, boron atoms are in pink, carbon atoms are in grey and hydrogen atoms are in white. (For interpretation of the references to colour in this figure legend, the reader is referred to the web version of this article.)

Table 1
Computed bond lengths (Å) for **A**, **B**, **C**, **TS1**, **TS2**, and **TS3** (see Chart 1 for atom numbering). Experimental values for **1** are given in parentheses for a comparison with **A**.

Distances	A	B	C	TS1 (A → B)	TS2 (A → C)	TS3 (A → C)
B1–B2	1.835 (1.794)	1.831	1.849	2.368	1.824	1.867
B2–B3	1.818 (1.788)	1.823	1.788	1.829	1.814	1.842
B3–B4	1.835 (1.799)	1.834	1.999	1.823	1.855	1.815
B4–B5	1.975 (1.966)	1.973	2.134	1.981	1.894	2.195
B5–B6	1.835 (1.795)	1.867	2.457	1.852	2.124	1.842
B6–B7	1.816 (1.796)	1.705	1.821	1.823	1.822	1.839
B7–B8	1.835 (1.816)	1.736	1.821	1.678	1.825	1.832
B9–B10	1.773 (1.772)	1.800	1.813	1.783	1.824	1.702
Ru–B5	2.223 (2.192)	2.257	2.297	2.198	3.164	2.255
Ru–B6	2.155 (2.127)	2.117	2.300	2.154	2.153	2.168
Ru–B7	2.155 (2.137)	2.148	2.200	2.239	2.143	2.125
Ru–B8	2.223 (2.118)	2.161	2.215	2.252	2.208	2.242
Ru–B9	2.266 (2.249)	2.279	2.223	2.232	2.195	2.815
Ru–B10	2.266 (2.240)	2.245	2.192	2.224	2.362	2.364
Ru–C(Cp)	2.351 (2.276)	2.331	2.355	2.342	2.321	2.312
Ru′–B1	2.223 (2.192)	2.235	2.265	2.159	2.243	2.229
Ru′–B2	2.155 (2.128)	2.152	2.193	2.105	2.154	2.139
Ru′–B3	2.228 (2.137)	2.158	2.184	2.177	2.161	2.146
Ru′–B4	2.228 (2.135)	2.227	2.371	2.240	2.208	2.301
Ru′–B9	2. 266 (2.255)	2.258	2.357	2.389	2.362	2.481
Ru′–B10	2.266 (2.246)	2.266	2.567	2.351	2.194	3.129
Ru′–C(Cp)	2. 349 (2.276)	2.351	2.341	2.345	2.331	2.341
B1–H11	1.374 (1.309)	1.361	1.377	2.067	1.277	1.392
B2–H12	1.356 (1.325)	1.361	1.347	1.538	1.331	1.353
B6–H13	1.356 (1.333)	1.359	1.418	1.334	1.357	1.299
B7–H14	1.316 (1.225)	1.303	1.366	–	1.278	1.302
H11–H12	1.912 (1.879)	1.945	1.939	0.801	1.845	1.955
H13–H14	1.942 (1.832)	–	1.944		1.932	1.957
B4–H15	1.237 (1.223)	–	1.342	–	1.336	1.
B5–H16	1.333 (1.321)	–	1.341	–	1.343	1.406
B5–H17	–	–	1.191	–	1.252	1.197
B6–H18	–	–	1.186	–	2.471	–
Ru′–H15	2.809 (2.811)	–	2.896	–	2.901	1.729
Ru–H16	2.836 (2.809)	–	2.990	–	2.891	1.917
Ru–H17	–	–	2.878	–	2.652	1.740
Ru′–H18	–	–	2.878	–	1.997	1.690
H15–H16	2.057 (2.061)	–	2.167	–	1.969	1.969
H17–H18	–	–	1.798	–	1.026	3.381
Ru–Ru′	4.105 (4.057)	4.064	4.264	4.077	4.206	4.929

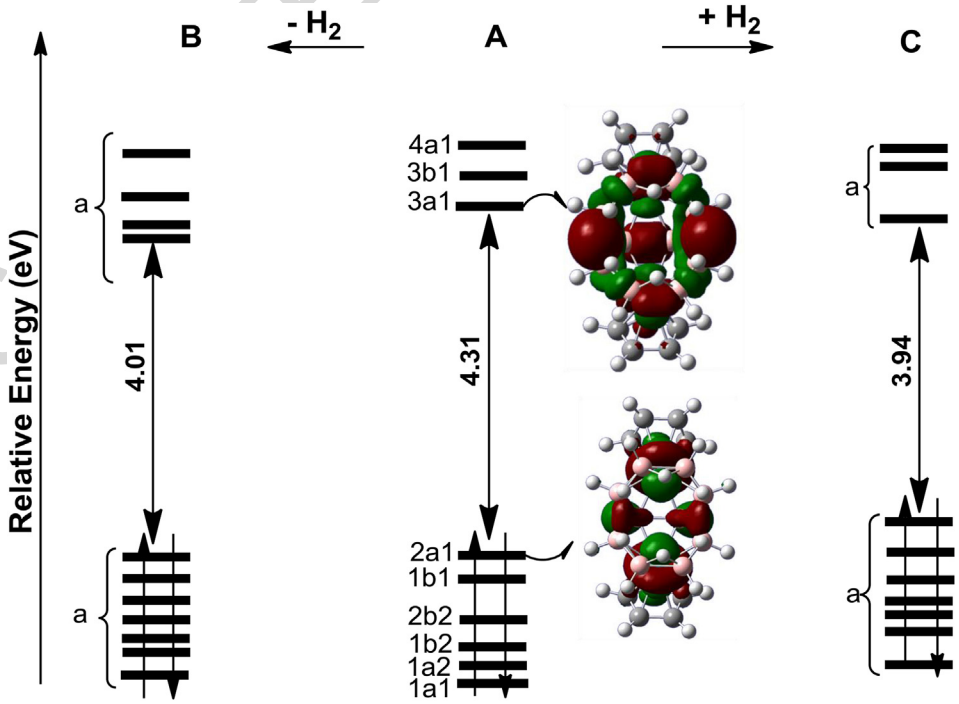

Fig. 2. MO diagrams of $Cp_2Ru_2B_{10}H_{16}$ **A** (middle), $Cp_2Ru_2B_{10}H_{14}$ **B** (left) and $Cp_2Ru_2B_{10}H_{18}$ **C** (right). Contour values for the HOMO ($2a_1$) and LUMO ($3a_1$) plots are ±0.12 $[e/bohr^3]^{1/2}$.

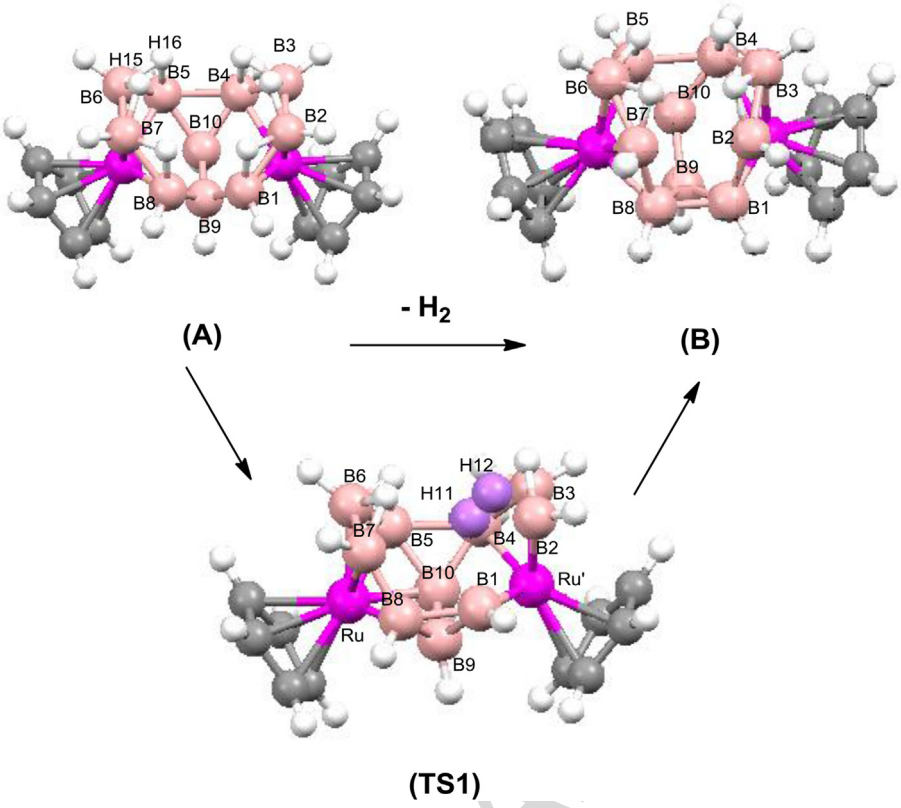

Fig. 3. Optimized molecular structures of **A**, **B** and **TS1**. The ruthenium atoms are shown in red, boron atoms are in pink, carbon atoms are in grey and hydrogen atoms are in white. H11 and H12 in **TS1** correspond to the added hydrogen atoms to **B**. (For interpretation of the references to colour in this figure legend, the reader is referred to the web version of this article.)

*Reaction path for addition H_2 to **A***

The reaction pathway for the addition of H_2 to **A** has also been studied. A dihydrogen molecule was added randomly at practically an infinite distance from **A**. The optimization yielded $Cp_2Ru_2B_{10}H_{18}$ (**C**) which is a stable energy minimum with a large HOMO–LUMO gap of 3.94 eV. The molecular structure of **C** is shown in Fig. 5 and the most relevant bond distances are listed in Table 1. In the structure one sees that the terminal atoms H17 and H18 are bound to B5 and B8, respectively. The Ru–B and B–B bond lengths change significantly upon addition of H_2 to **A**. The Ru–B6 bond is elongated by 30 pm to 2.456 Å which changes the metal coordination. The Ru–Ru′ distance increases by 16 pm to 4.264 Å and the B5–B6 bond breaks as the distance is 2.457 Å. In **C**, the long distance of 1.798 Å between the two incoming hydrogen (H17 and H18) indicates that the H–H bond dissociates. The Ru′–B10 distance of 2.567 Å is much longer than in **A** and **B**. The structural changes occur mainly in the borane cage leading to its opening upon H_2 addition.

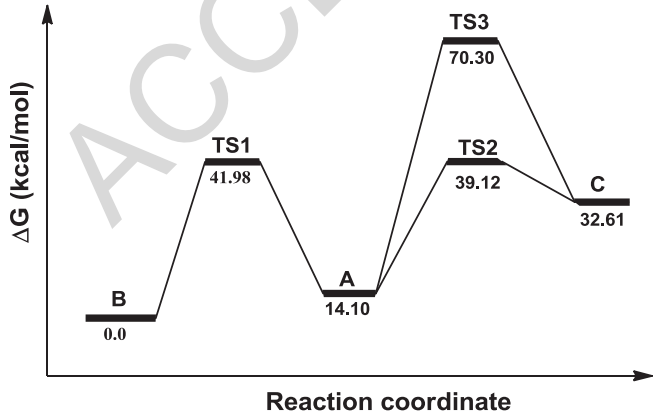

Fig. 4. Energy profile of the hydrogenation. The relative energies of the reactants, products of **A**, **B** and **C** through the dehydrogenation in **B** → **A** (left side) and for hydrogenation in **A** → **C** processes (right side). The transition states (**TS1**, **TS2** and **TS3**) are given.

By using the IRC procedure, we found transitions states (**TS2** and **TS3**) that connect **A** and **C**, both with large HOMO–LUMO gaps of 4.03 eV and 3.02 eV, respectively. Their optimized bond distances are listed in Table 1. **TS2** has a short bond distance of 1.026 Å between the hydrogen atoms of the incoming H_2 molecule (H17 and H18) which has η^2 coordination to B9. The B9–H17 and B9–H18 distances are 1.332 Å and 1.319 Å, respectively, as also observed in Kubas' complexes [19]. The B5–B6 bond of 2.124 Å is longer than for **A**. **TS2** is 6.5 kcal/mol above **C**. The Gibbs activation energy for the **A** + H_2 to **C** through **TS2** is 25 kcal/mol. The second transition state (**TS3**) has metal hydride bonds, Ru′–H18 and Ru–H17 distances of 1.690 Å and 1.740 Å, respectively. In **TS3**, the B4–B5 distance of 2.195 Å is slightly longer than the rest of the B–B bonds. Thus, the incoming H_2 bond dissociates forming metal hydrides in **TS3**. Chaudret et al. have previously reported that short Ru–H bond lengths are common in ruthenium–hydrogen chemistry [22–25].

Activation energy

The Gibbs free energies (ΔG) for **TS1** and **TS2** indicate that the elimination/addition reaction of H_2 occurs through activation of the σ_{H-H} bond, whereas the higher activation energy of 70.3 kcal/mol for **TS3** implies that oxidative addition on Ru is not the reaction

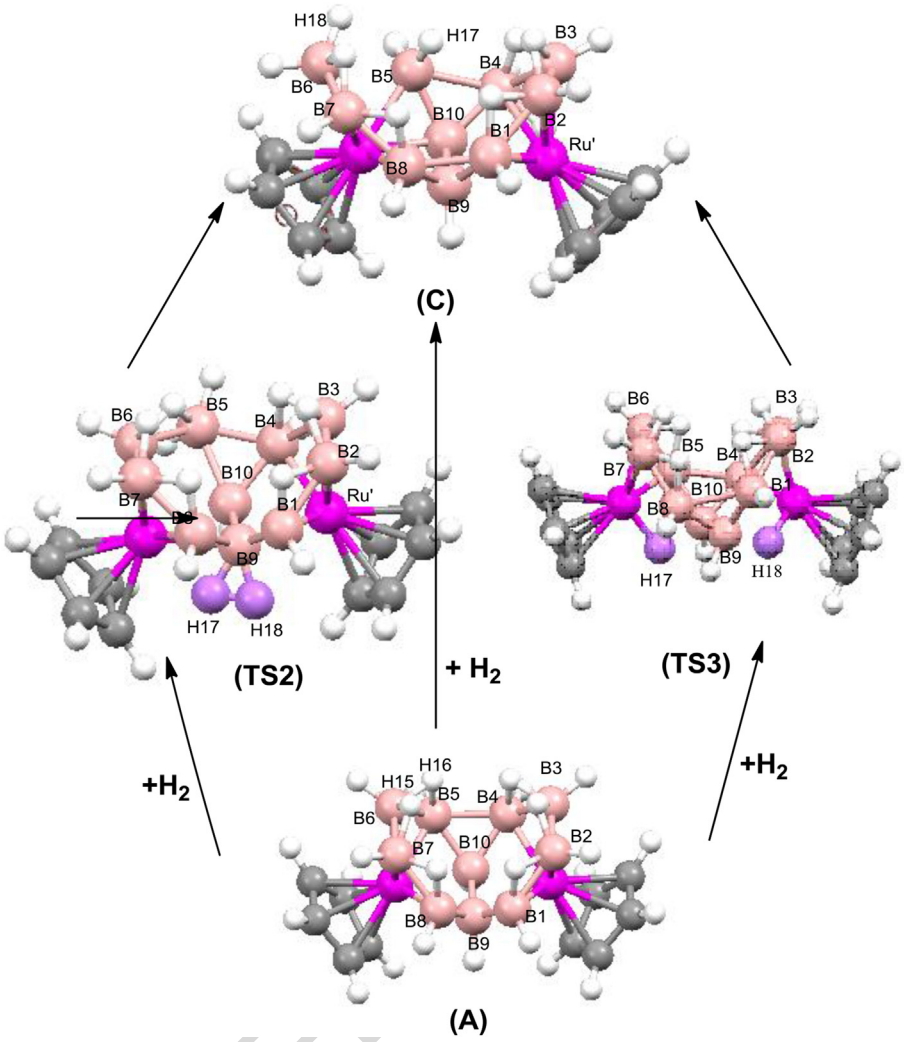

Fig. 5. The optimized structures of **C** ([$Cp_2Ru_2B_{10}H_{18}$]) and of the two transition states (**TS2** and **TS3**) involved in the hydrogenation process (**A** → **C**). The ruthenium atoms are presented by red balls. The pink ones are B. C is grey and H is white. The purple atoms are the hydrogen atoms added to **A** in the hydrogenation reaction. (For interpretation of the references to colour in this figure legend, the reader is referred to the web version of this article.)

pathway of the hydrogenation addition reaction of **A**. The reason for this high-energy barrier is basically the energy level crossing of the lone pair orbital and the antibonding σ^* orbital of H_2 [22]. Due to the relatively low activation barriers for **TS1** and **TS2**, we assume that a fast reversible equilibrium might occur through the hydrogenation and dehydrogenation processes via **TS1** and **TS2**. The weak interaction of H_2 with the borane ligand might be a key step for achieving a fast and controlled H_2 uptake [15,36].

To probe the solvent effect, we carried out single-point calculations of the activation energy of the studied clusters. In the PCM calculations with toluene as solvent, we obtained a lowering in the energy barrier of 3–4 kcal/mol for the studied reactions, which agrees with our previous work [19]. The small reduction in the activation energy suggests the solvent does not change the pathway of the dehydrogenation/hydrogenation reaction, whereas slightly lower barriers are obtained when solvent effects are taken into account.

Related reactions

The computational study of the cluster stability and the activation of the H_2 bond by the ruthenium cluster were extended to the recently synthesized ruthenaboranes $Cp^*_2Ru_2B_8H_{14}$ (**2**) and $Cp^*_2Ru_2B_8H_{12}$ (**3**) [16]. In the previous section, we found that the hydrogenation and dehydrogenation do not change substantially the borane structure of **1**. We therefore carried out similar calculations on models **D** and **E** used to mimic compounds **2** and **3** to check if such a behaviour is general in metallaborane chemistry. In these models, the Cp^* units in **2** and **3** were replaced by Cp ligands.

The $Cp_2Ru_2B_8H_{14}$ structure

The optimized $Cp_2Ru_2B_8H_{14}$ model cluster **D** is drawn in Fig. 6. Selected bond distances are gathered in Table 2. The molecular structure of **D** belongs to the C_{2h} point group, which is also the approximate symmetry of the crystal structure of the methyl substituted relative (**2**) [36]. The optimized structure of $Cp_2Ru_2B_8H_{14}$ exhibits slightly longer Ru–B and longer Ru–C(Cp) distances than observed in $Cp^*_2Ru_2B_8H_{14}$. The metal is pentacoordinated to the borane. **D** has a HOMO–LUMO gap of 3.52 eV. The Ru–Ru distance of 3.952 Å is somewhat longer than the experimental one of 3.897 Å [16]. The average of B–B and Ru–B bond lengths of 1.833 Å and 2.191 Å, respectively, are also somewhat longer than the experimental ones, which are given in parenthesis in Table 2.

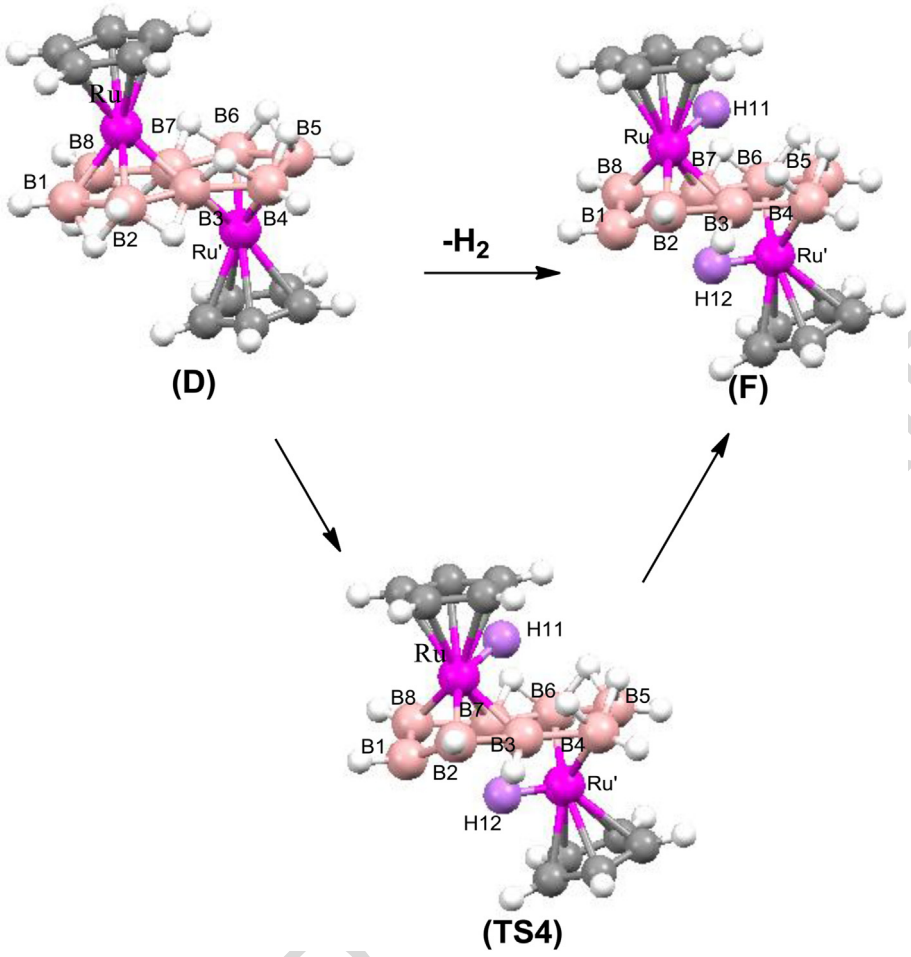

Fig. 6. Molecular structures of $[Cp_2Ru_2(B_8H_{14})]$ (**D**), $[Cp_2Ru_2(B_8H_{12})]$ (**F**) and **TS4**. The red balls are Ru and the pink ones are B. C is grey and H is white. (For interpretation of the references to colour in this figure legend, the reader is referred to the web version of this article.)

Different H_2 elimination reactions of $[Cp_2Ru_2(B_8H_{14})]$ **D** were investigated. The most stable cluster structure for $Cp_2Ru_2B_8H_{12}$ (**F**) has metal hydride bonds (see Fig. 6). The most relevant bond distances for **F** are given in Table 2. The H_2 elimination reaction of **D** yielding **F** leads to some structural changes, which mainly occur in the boron skeleton. The B1–B2 and B7–B8 bonds become shorter. The Ru–Ru′ distance of 3.837 Å is slightly shorter than for **D**. The cluster **F** has two short metal–hydride bonds whose distances are

Table 2
Selected optimized bond distances for **D**, **E**, **F**, **G**, **TS4** and **TS5**. The bond lengths are given in Å. Experimental values are given in parentheses.

$M_2Cp_2B_8H_n$ (n=)	**D** (14)	**E** (12)	**F** (12)	**G** (14)	**TS4** (**D** → **F**) (14)	**TS5** (**E** → **G**) (14)
B1–B2	1.834 (1.820)	1.783 (1.778)	1.738	2.015	1.841	2.102
B2–B3	1.824 (1.823)	1.774 (1.772)	1.867	*1.775*	1.801	1.785
B2–B4	1.834 (1.827)	2.068 (2.014)	1.712	2.031	1.803	2.041
B4–B5	1.834 (1.827)	1.829 (1.817)	1.901	*1.810*	1.750	1.833
B5–B6	1.824 (1.820)	1.822 (1.806)	1.842	1.801	1.751	1.806
B7–B8	1.834 (1.827)	1.794 (1.799)	1.811	1.782	1.802	1.725
Ru–B1	2.141 (2.107)	2. 285 (2.206)	2.319	2.591	2.312	2.634
Ru–B2	2.128 (2.111)	3.333 (3.288)	2.071	2.192	2.215	3.701
Ru–B3	2.175 (2.152)	2.324 (2.288)	2.123	2.156	2.291	2.412
Ru–B7	2.175 (2.149)	2.136 (2.114)	2.132	2.135	2.294	2.196
Ru–B8	2.128 (2.106)	3.179 (3.141)	2.124	2.167	2.151	3.221
Ru–C(Cp)	2.334 (2.251)	2.321 (2.241)	2.281	2.331	2.331	2.315
Ru′–B3	2.175 (2.149)	3.287 (3.271)	2.304	2.104	2.341	3.241
Ru′–B4	2.128 (2.106)	2.200 (2.173)	2.165	2.165	2.181	2.271
Ru′–B5	2.141 (2.107)	2.184 (2.150)	2.181	2.192	2.155	2.186
Ru′–B6	2.128 (2.111)	2.115 (2.108)	2.168	2.216	2.151	2.126
Ru′–B7	2. 175 (2.152)	2.132 (2.121)	2.305	–	2.281	2.132
Ru′–B8	2.341 (2.249)	2.281 (2.238)	2.811	–	2.901	2.321
Ru′–C(Cp)	2.321 (2.331)	2.281 (2.271)	2.331	–	2.351	2.345
Ru–H11	–	1.702 (1.602)	1.781	1.695	1.721	1.795
Ru′–H12	–	–	1.891	1.663	1.819	1.763
Ru–Ru′	3.952 (3.897)	2.901 (2.889)	3.836	2.866	3.261	3.028

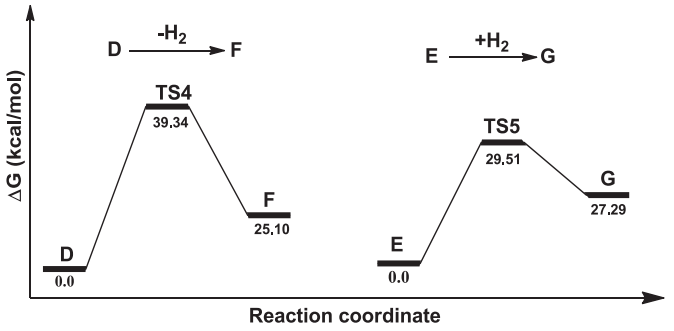

Fig. 7. Relative energies between the optimized structures **D** and **F** and between **E** and **G**.

1.781 Å and 1.891 Å for Ru—H11 and Ru′—H12, respectively. The Ru—B1 and Ru′—B3 bonds break leading to a preservation of the 18-electron rules for the complex. The energy difference between **D** and **F** is 25.1 kcal/mol (see Fig. 7). In the search for the transition state of the H_2 elimination reaction from **D** to **F**, we found one transition state (**TS4**) involving metal—hydride bonds. The Ru—H11 and Ru′—H12 distances are 1.721 Å and 1.819 Å, respectively. The activation barrier of **TS4** from **D** to **F** and from **F** to **D** are 39.3 kcal/mol and 14.2 kcal/mol respectively. The calculations suggest that the hydrogenation reaction does not involve any oxidative addition or reductive elimination in this cluster. For **F** and **TS4**, the Cp—M bonding does not change much resulting in a similar structure as for **D**.

The $Cp_2Ru_2(B_8H_{12})$ structure

Since the crystallographic [16] and electronic [17] structures of $(C_5Me_5)_2Ru_2B_8H_{12}$ (**3**) are known, we focus here on the hydrogenation reaction with $Cp_2Ru_2B_8H_{12}$ (**E**) as starting structure for the calculations. The molecular structure of **E** was also optimized. Selected bond distances are compared to experimental values in Table 2. The largest deviations between calculated and observed bond distances for **E** occur for Ru—B2, Ru′—B3, and B2—B4. **E** has only one short hydride—metal bond, namely Ru—H11 which is 1.702 Å long. The Ru—Ru′ distance in **E** of 2.889 Å is short as compared to the experimental one.

We also studied the H_2 addition reaction of **E** yielding the stable structure $Cp_2Ru_2B_8H_{14}$, which is labelled **G** in Fig. 8. The most relevant bond lengths of the optimized structure of **G** are given in Table 2. The optimization of the **G** yielded a structure with two metal—hydride bonds of 1.695 Å and 1.663 Å and broken Ru—B bonds. The transition state (**TS5**) between **E** and **G** was obtained using IRC. **TS5** has also two short metal—hydride bonds of 1.721 Å and 1.819 Å and broken Ru—B bonds. The bond distances are given in Table 2 and the molecular structure is shown in Fig. 8. The energy levels in Fig. 7 show that **G** is 27.3 kcal/mol higher in energy than **E** and **TS5** is 29.5 kcal/mol above **E** and only 2.2 kcal/mol above **G**. The obtained energy barrier at **TS5** suggests that **E** and **G** might be a good cluster pair for reversible hydrogenation/dehydrogenation reactions and storage of H_2.

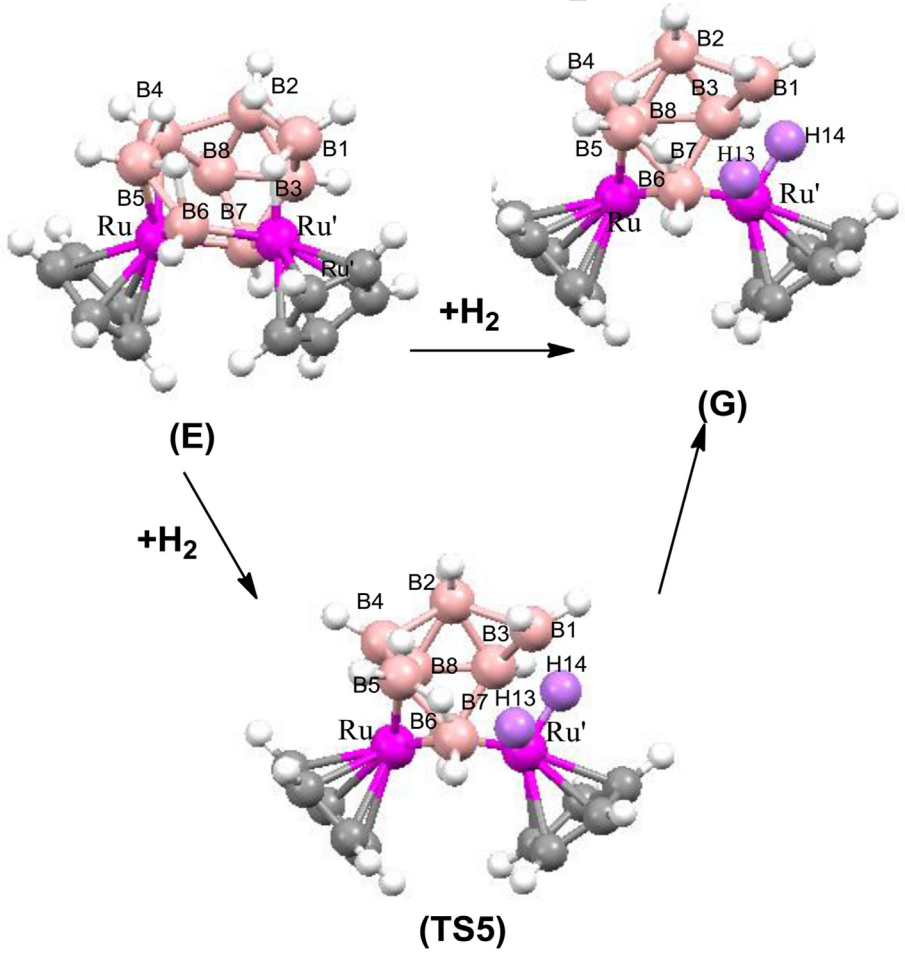

Fig. 8. B3LYP-optimized structures of $[Cp_2Ru_2(B_8H_{12})]$ (**E**), $[Cp_2Ru_2(B_8H_{14})]$ (**G**) and **TS5**. The red balls are Ru and the pink ones are B. C is grey and H is white. The purple atoms are the hydrogen atoms involved in the hydrogenation process. (For interpretation of the references to colour in this figure legend, the reader is referred to the web version of this article.)

Conclusions

Hydrogenation and dehydrogenation processes of ruthenaborane clusters have been studied computationally at the DFT/B3LYP level. Calculations show different bonding modes of the added H_2 molecule to the investigated clusters.

Optimization of the ruthenaborane clusters yielded both η^2-H_2 coordinated as well as formation of metal–hydride (Ru–H) bonds. Activation pathways of the H–H bond by ruthenaboranes were also analysed. Calculations of the energy profiles yielded H_2 addition and elimination energies of 14–27 kcal/mol for the studied (**A**, **B**, **D** and **E**) clusters. The calculated H_2 elimination energy of **D** yielding **F** is 25 kcal/mol. The obtained results indicate that molecular hydrogen can be added to electron-deficient metallaborane clusters with high hydride content such as $Cp^*_2Ru_2B_{10}H_{16}$ and $Cp^*_2Ru_2B_8H_{12}$. However, whereas the free energies of the H_2 uptake reactions appear to be nearly acceptable, the activations barrier are too large for expecting the reactions to occur at room temperature or under moderate heating. Work is in progress in our group to design related systems with lower activation barriers and reaction free energies. Nevertheless, this study suggests that these kinds of clusters may be a good conceptual starting point for the development of metal–hydride based materials suitable for hydrogen storage or of molecular catalysts for hydrogen storage processes [37,38].

Acknowledgement

We thank the CNRS (France), the CNRST (Morocco) Convention: Chimie:13-10, the Indo-French Centre for Promotion of Advanced Research (IFCPAR, Project No. 4405-1) and the University of Helsinki for their financial support. This research was also supported by the Academy of Finland through Project 137460 and its Computational Science Research Programme (LASTU/258258).

Appendix A. Supplementary data

Supplementary data related to this article can be found at http://dx.doi.org/10.1016/j.jorganchem.2014.03.001.

References

[1] J. Graetz, Chem. Soc. Rev. 38 (2009) 73.
[2] S. Orimo, Y. Nakamori, J.R. Eliseo, A. Zuttel, C.M. Jensen, Chem. Rev. 107 (2007) 4111.
[3] C.W. Hamilton, R.T. Baker, A. Staubitz, I. Manners, Chem. Soc. Rev. 38 (2009) 279.
[4] A.W.C. van der Berg, C.O. Arean, Chem. Commun. (2008) 668.
[5] S.A. Shevlin, Z.X. Guo, Chem. Soc. Rev. 38 (2009) 211.
[6] T. Matsunagaa, F. Buchtera, K. Miwac, S. Towatac, S. Orimod, A. Zuttel, Renew. Energy 33 (2008) 193.
[7] J. Yang, A. Sudik, D.J. Siegel, D. Halliday, A. Drews, R.O. Carter III, C. Wolverton, G.J. Lewis, J.W.A. Sachtler, J.J. Low, S.A. Faheem, D.A. Lesch, V. Ozolins, Angew. Chem. Int. Ed. 47 (2008) 882.
[8] D.A. Dixon, M. Gutowski, J. Phys. Chem. A 109 (2005) 5129.
[9] Y. Nakamori, H.-W. Li, M. Matsuo, K. Miwa, S. Towata, S. Orimo, J. Phys. Chem. Solids 69 (2008) 2292.
[10] F.H. Stephens, V. Ponns, T.R. Baker, Dalton Trans. (2007) 2613.
[11] U. Eberle, M. Felderhoff, F. Sch∏th, Angew. Chem. Int. Ed. 48 (2009) 6608.
[12] F. de Montigny, R. Macias, B.C. Noll, T.P. Fehlner, K. Costuas, J.-Y. Saillard, J.-F. Halet, J. Am. Chem. Soc. 129 (2007) 3392.
[13] S.B. Sun, M.L. McKee, Inorg. Chem. 52 (2013) 5962.
[14] S. Ghosh, B.C. Noll, T.P. Fehlner, Angew. Chem. Int. Ed. 44 (2005) 2916.
[15] M. Rochdi, H. Rabaa, S. Ghosh, J.-Y. Saillard, J.F. Halet, Polyhedron 43 (2012) 31.
[16] S. Ghosh, A.M. Beatty, T.P. Fehlner, Angew. Chem. Int. Ed. 42 (2003) 4678.
[17] L. Guennic, H. Jiao, S. Kahal, J.-Y. Saillard, J.-F. Halet, S. Ghosh, M. Shang, A.M. Beatty, A.L. Rheingold, T.P. Fehlner, J. Am. Chem. Soc. 126 (2004) 3203.
[18] M.T. Kelly, Struct. Bonding 141 (2011) 169.
[19] G.J. Kubas, Metal Dihydrogen and σ Bond Complexes: Structure, Theory and Reactivity, Kluwer Academic/Plenium, New York, 2001.
[20] G.J. Kubas, Chem. Rev. 107 (2007) 2613.
[21] H. Rabaâ, J.-Y. Saillard, R. Hoffmann, J. Am. Chem. Soc. 108 (1986) 4327.
[22] A.K. Kandalam, B. Kiran, P. Jena, J. Phys. Chem. C 112 (2008) 6181.
[23] G. Alcaraz, M. Grellier, S. Sabo-Etienne, Acc. Chem. Res. 42 (2009) 1640.
[24] I. Atheaux, F. Delpech, B. Donnadieu, S. Sabo-Etienne, B. Chaudret, K. Hussein, J.C. Barthelat, T. Braun, S.B. Duckett, R.N. Perutz, Organometallics 21 (2002) 5347.
[25] T. Arliguie, B. Chaudret, R.H. Morris, A. Sella, Inorg. Chem. 27 (1988) 598.
[26] M.J. Frisch, et al., Gaussian 09, Revision A.1, Gaussian, Inc., Wallingford CT, 2009.
[27] C. Lee, W. Yang, R.G. Parr, Phys. Rev. B 37 (1988) 785.
[28] A.D. Becke, J. Chem. Phys. 98 (1993) 5648.
[29] W.J. Stevens, H. Basch, M. Krauss, J. Chem. Phys. 81 (1984) 6026.
[30] C. Peng, H.B. Schlegel, J. Israel, J. Chem. Phys. 33 (1993) 449.
[31] C. Peng, P.Y. Ayala, H.B. Schlegel, M.J. Frisch, J. Comput. Chem. 17 (1996) 49.
[32] G. Scalmani, M.J. Frisch, J. Chem. Phys. 132 (2010) 114110.
[33] T.P. Fehner, J.-F. Halet, J.-Y. Saillard, Molecular Cluster, Cambridge Univ. Press., Cambridge, UK, 2007.
[34] D.M.P. Mingos, D.J. Wales, Introduction to Cluster Chemistry, Prentice-Hall, Englewood Cliffs, 1990.
[35] M. Touil, B. Bechem, A.S.K. Hashmi, B. Engels, M.A. Omary, H. Rabaâ, J. Mol. Struct. Theochem. 975 (2010) 21.
[36] B. Boucher, S. Ghosh, J.-F. Halet, S. Khalal, J.-Y. Saillard, J. Organomet. Chem. 721 (2012) 167.
[37] R.D. Adams, B. Captain, Angew. Chem. Int. Ed. 47 (2008) 252.
[38] R.H. Crabtree, Organometallics 30 (2011) 17.